Measurement of Muon Neutrino Quasielastic Scattering on a Hydrocarbon Target at $E_\nu \sim 3.5$ GeV

G. A. Fiorentini,[1] D. W. Schmitz,[2,3] P. A. Rodrigues,[4] L. Aliaga,[5,6] O. Altinok,[7] B. Baldin,[3] A. Baumbaugh,[3] A. Bodek,[4] D. Boehnlein,[3] S. Boyd,[8] R. Bradford,[4] W. K. Brooks,[9] H. Budd,[4] A. Butkevich,[10] D. A. Martinez Caicedo,[1,3] C. M. Castromonte,[1] M. E. Christy,[11] H. Chung,[4] J. Chvojka,[4] M. Clark,[4] H. da Motta,[1] D. S. Damiani,[5] I. Danko,[8] M. Datta,[11] M. Day,[4] R. DeMaat,[3,*] J. Devan,[5] E. Draeger,[12] S. A. Dytman,[8] G. A. Díaz,[6] B. Eberly,[8] D. A. Edmondson,[5] J. Felix,[13] L. Fields,[14] T. Fitzpatrick,[3,*] A. M. Gago,[6] H. Gallagher,[7] C. A. George,[8] J. A. Gielata,[4] C. Gingu,[3] B. Gobbi,[14,*] R. Gran,[12] N. Grossman,[3] J. Hanson,[4] D. A. Harris,[3] J. Heaton,[12] A. Higuera,[13] I. J. Howley,[5] K. Hurtado,[1,15] M. Jerkins,[16] T. Kafka,[7] J. Kaisen,[4] M. O. Kanter,[5] C. E. Keppel,[11,†] J. Kilmer,[3] M. Kordosky,[5] A. H. Krajeski,[5] S. A. Kulagin,[10] T. Le,[17] H. Lee,[4] A. G. Leister,[5] G. Locke,[17] G. Maggi,[9,‡] E. Maher,[18] S. Manly,[4] W. A. Mann,[7] C. M. Marshall,[4] K. S. McFarland,[4,3] C. L. McGivern,[8] A. M. McGowan,[4] A. Mislivec,[4] J. G. Morfín,[3] J. Mousseau,[19] D. Naples,[8] J. K. Nelson,[5] G. Niculescu,[20] I. Niculescu,[20] N. Ochoa,[6] C. D. O'Connor,[5] J. Olsen,[3] B. Osmanov,[19] J. Osta,[3] J. L. Palomino,[1] V. Paolone,[8] J. Park,[4] C. E. Patrick,[14] G. N. Perdue,[4] C. Peña,[9] L. Rakotondravohitra,[3,§] R. D. Ransome,[17] H. Ray,[19] L. Ren,[8] C. Rude,[12] K. E. Sassin,[5] H. Schellman,[14] R. M. Schneider,[5] E. C. Schulte,[17,‖] C. Simon,[21] F. D. Snider,[3] M. C. Snyder,[5] J. T. Sobczyk,[22,3] C. J. Solano Salinas,[15] N. Tagg,[23] W. Tan,[11] B. G. Tice,[17] G. Tzanakos,[24,*] J. P. Velásquez,[6] J. Walding,[5,¶] T. Walton,[11] J. Wolcott,[4] B. A. Wolthuis,[5] N. Woodward,[12] G. Zavala,[13] H. B. Zeng,[4] D. Zhang,[5] L. Y. Zhu,[11] and B. P. Ziemer[21]

(MINERvA Collaboration)

[1]*Centro Brasileiro de Pesquisas Físicas, Rua Dr. Xavier Sigaud 150, Urca, Rio de Janeiro, Rio de Janeiro 22290-180, Brazil*
[2]*Enrico Fermi Institute, University of Chicago, Chicago, Illinois 60637, USA*
[3]*Fermi National Accelerator Laboratory, Batavia, Illinois 60510, USA*
[4]*University of Rochester, Rochester, New York 14610, USA*
[5]*Department of Physics, College of William and Mary, Williamsburg, Virginia 23187, USA*
[6]*Sección Física, Departamento de Ciencias, Pontificia Universidad Católica del Perú, Apartado 1761, Lima, Perú*
[7]*Physics Department, Tufts University, Medford, Massachusetts 02155, USA*
[8]*Department of Physics and Astronomy, University of Pittsburgh, Pittsburgh, Pennsylvania 15260, USA*
[9]*Departamento de Física, Universidad Técnica Federico Santa María, Avenida España 1680, Casilla 110-V, Valparaíso, Chile*
[10]*Institute for Nuclear Research of the Russian Academy of Sciences, 117312 Moscow, Russia*
[11]*Hampton University, Deptartment of Physics, Hampton, Virginia 23668, USA*
[12]*Department of Physics, University of Minnesota-Duluth, Duluth, Minnesota 55812, USA*
[13]*Campus León y Campus Guanajuato, Universidad de Guanajuato, Lascurain de Retana No. 5, Colonia Centro Guanajuato, 36000 Guanajuato, México*
[14]*Northwestern University, Evanston, Illinois 60208, USA*
[15]*Universidad Nacional de Ingeniería, Apartado 31139, Lima, Perú*
[16]*Department of Physics, University of Texas, 1 University Station, Austin, Texas 78712, USA*
[17]*Rutgers, The State University of New Jersey, Piscataway, New Jersey 08854, USA*
[18]*Massachusetts College of Liberal Arts, 375 Church Street, North Adams, Massachusetts 01247, USA*
[19]*Department of Physics, University of Florida, Gainesville, Florida 32611, USA*
[20]*James Madison University, Harrisonburg, Virginia 22807, USA*
[21]*Department of Physics and Astronomy, University of California, Irvine, Irvine, California 92697-4575, USA*
[22]*Institute of Theoretical Physics, Wrocław University, 50-204 Wrocław, Poland*
[23]*Department of Physics, Otterbein University, 1 South Grove Street, Westerville, Ohio 43081, USA*
[24]*Department of Physics, University of Athens, GR-15771 Athens, Greece*

(Received 9 May 2013; published 11 July 2013)

We report a study of ν_μ charged-current quasielastic events in the segmented scintillator inner tracker of the MINERvA experiment running in the NuMI neutrino beam at Fermilab. The events were selected by requiring a μ^- and low calorimetric recoil energy separated from the interaction vertex. We measure

the flux-averaged differential cross section, $d\sigma/dQ^2$, and study the low energy particle content of the final state. Deviations are found between the measured $d\sigma/dQ^2$ and the expectations of a model of independent nucleons in a relativistic Fermi gas. We also observe an excess of energy near the vertex consistent with multiple protons in the final state.

DOI: 10.1103/PhysRevLett.111.022502 PACS numbers: 21.10.−k, 13.15.+g, 25.30.Pt

Charged-current neutrino quasielastic (QE) scattering, $\nu_\mu n \to \mu^- p$, distinguishes neutrino flavor and is valuable for neutrino oscillation experiments at energies near 1 GeV where it is responsible for a large fraction of the total reaction cross section [1–4]. For free nucleons, the scattering process may be described by the standard theory of weak interactions with the inclusion of nucleon form factors [5]. Electron scattering [6] and neutrino scattering on deuterium [7,8] determine the most important form factors with good precision [9]. However, neutrino oscillation experiments typically use detectors made of heavier nuclei such as carbon [4,10], oxygen [11], iron [12], or argon [13,14] where interactions with nucleons are modified by the nuclear environment. These effects are commonly modeled using a relativistic Fermi gas (RFG) [15,16] description of the nucleus as quasifree, independent nucleons with Fermi motion in a uniform binding potential. Neutrino interaction generators [17–21] additionally simulate interactions of final state hadrons inside the target nucleus. The MiniBooNE experiment recently observed that this prescription, utilizing the free deuterium value for the axial form factor, does not accurately describe their measurements of quasielastic scattering of neutrinos and antineutrinos on a hydrocarbon target [22,23].

The RFG approach may be supplemented by accounting for correlations between nucleons within the nucleus. Evidence for these correlations has been observed in electron-nucleus scattering [24]. Processes that produce multiple final state nucleons are thought to lead to enhancements in the cross section [25–27]. These contributions are modeled using different approaches [28–30] which produce qualitatively similar, though not quantitatively identical, results. The RFG model may also be replaced by an alternate spectral function (SF) model that calculates the joint probability distribution of scattering off a nucleon of given momentum and binding energy inside a nucleus [31]. These nuclear effects may be significant for oscillation experiments seeking to measure the neutrino mass hierarchy and CP violation [32–34].

In this Letter, we report the first study of muon neutrino quasielastic interactions at energies between 1.5 and 10 GeV from the MINERvA experiment, which uses a finely segmented scintillator detector at Fermilab to measure muon neutrino interactions on nuclear targets. The analysis technique is similar to the one employed to study the antineutrino reaction [35]. The signal has a μ^- in the final state along with one or more nucleons (typically with a leading proton), and no mesons. We reject events in which mesons are produced by requiring that the hadronic system recoiling against the muon has a low energy. That energy is measured in two spatial regions. The vertex energy region corresponds to a sphere around the vertex with a radius sufficient to contain a proton (pion) with 225 (100) MeV kinetic energy. This region is sensitive to low energy protons which could arise from correlations among nucleons in the initial state or final state interactions of the outgoing hadron inside the target nucleus [36]. We do not use the vertex energy in the event selection but study it for evidence of multinucleon processes. The recoil energy region includes energy depositions outside of the vertex region and is sensitive to pions and higher energy nucleons. We use the recoil energy to estimate and remove inelastic backgrounds.

The MINERvA detector was exposed to the NuMI neutrino beam at Fermilab, configured for this analysis to produce a beam consisting of >95% ν_μ at the peak energy of 3 GeV. The neutrino flux is predicted using a GEANT4-based simulation tuned to hadron production data [37] as described in Ref. [35]. This analysis uses data taken between March and July 2010 with 9.42×10^{19} protons on target.

The MINERvA detector consists of a fine-grained scintillator tracker surrounded by electromagnetic and hadronic calorimeters [38,39]. The detector enables reconstruction of the neutrino interaction point, the tracks of outgoing charged particles, and the calorimetric reconstruction of other particles produced in the interaction. MINERvA is located 2 m upstream of the MINOS near detector [12], which is used to reconstruct the momentum and charge of muons. The hadronic energy scale is set using data from through-going muons and a scaled down MINERvA detector exposed to a hadron test beam [39]. The detector's performance is simulated by a GEANT4-based hit-level simulation and a readout model tuned to match the data [39]. Event pileup causes a decrease in the muon track reconstruction efficiency which we studied in both MINERvA and MINOS by projecting tracks found in one of the detectors to the other and measuring the misreconstruction rate. This resulted in a −9.1% (−4.8%) correction to the simulated efficiency for muons with momenta below (above) 3 GeV/c in MINOS. Neutrino interactions in the detector are simulated using the GENIE neutrino event generator [17]. Details of the cross-section models and associated parameters are described in Ref. [35].

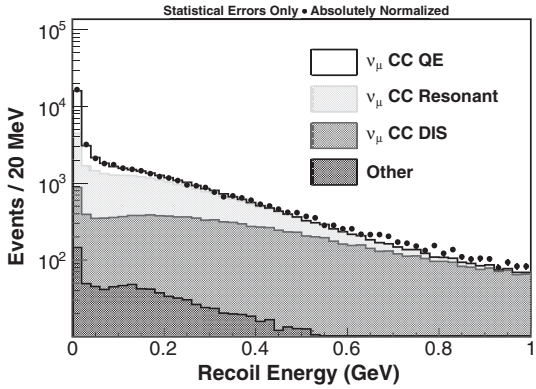

FIG. 1. The measured recoil energy distribution in the data (solid circles) and the predicted composition of signal and background. Backgrounds from charged-current (CC) baryon resonance production (light gray), continuum or deep-inelastic scattering (DIS) (dark gray), and other sources (black), such as coherent pion production, are shown. The fraction of signal before requiring low recoil energy is 0.29.

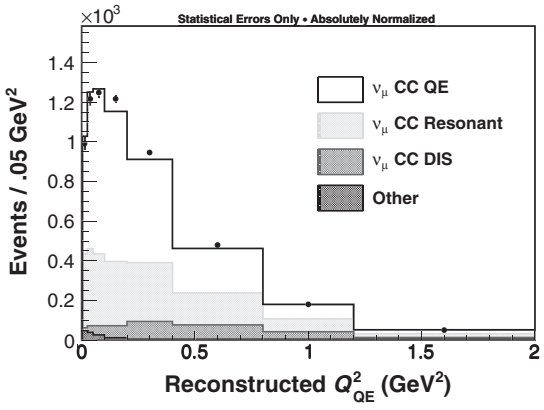

FIG. 2. The measured $Q^2_{\rm QE}$ distributions in the data and the simulation, before correcting for detector resolution and acceptance. The fraction of signal in this sample is 0.49, and 47% of signal events in our fiducial volume pass all selections.

Event reconstruction and selection for this analysis is nearly identical to that used in the MINERvA antineutrino quasielastic measurement [35] with small modifications to account for the likelihood of a leading proton in the final state instead of a neutron. We require events to have a μ^- originating in the 5.57 metric ton fiducial volume and assign remaining clusters with energies >1 MeV to the recoiling hadronic system. The aforementioned vertex region corresponds to a sphere with 30 g/cm^2 of material centered on the vertex. The recoil system outside the vertex region is required to have ≤ 2 isolated groups of spatially contiguous energy depositions [40].

The neutrino energy and the square of the four momentum transferred to the nucleus, $Q^2_{\rm QE}$, are estimated from the muon momentum and angle using a quasielastic hypothesis, as in the antineutrino analysis [35]. The binding energy correction is taken to be $+34$ MeV instead of $+30$ MeV used in Ref. [35] due to Coulomb corrections [41], and the proton and neutron masses are interchanged.

Figure 1 shows that the quasielastic signal preferentially populates lower recoil energies. However, since the proton's kinetic energy is $\approx Q^2/2M_{\rm neutron}$ for quasielastic scattering, the recoil energy is expected to scale with the momentum transfer as the final state proton becomes increasingly energetic and escapes the vertex region. We account for this by varying a cut on the maximum allowed recoil energy as a function of $Q^2_{\rm QE}$ to assure 95% signal efficiency in each $Q^2_{\rm QE}$ bin.

The background in each $Q^2_{\rm QE}$ bin is estimated from the data by fitting the relative normalizations of signal and background recoil energy distributions whose shapes are taken from the simulation. This procedure reduces the relative background prediction by 15% below $Q^2_{\rm QE}$ of 0.8 GeV^2 and 5% between 0.8 and 2.0 GeV^2. The purity of the resulting sample ranges from 65% at low $Q^2_{\rm QE}$ to 40% at higher $Q^2_{\rm QE}$. Figure 2 compares the $Q^2_{\rm QE}$ distribution of the 29 620 events which satisfy the selection criteria to the simulation after rescaling the background according to the fit. The cross section as a function of $Q^2_{\rm QE}$ is extracted by subtracting the backgrounds, correcting for detector resolution and acceptance, and dividing by the number of neutrons in the fiducial volume $(1.65 \pm 0.02) \times 10^{30}$ and by the flux, as described in Ref. [35]. The total neutrino flux integrated between 1.5 and 10 GeV is estimated by the simulation to be $2.91 \times 10^{-8}/\text{cm}^2$ per proton on target [42].

The same systematic uncertainties which affect the antineutrino analysis [35] are evaluated in this analysis. Table I shows a summary of systematic uncertainties on $d\sigma/dQ^2_{\rm QE}$. The largest uncertainties on the absolute cross section come from the neutrino flux and the muon momentum scale. However, the flux uncertainty is largely independent of $Q^2_{\rm QE}$, so comparisons of the shape of $d\sigma/dQ^2_{\rm QE}$ to scattering model predictions are relatively insensitive to

TABLE I. Fractional systematic uncertainties on $d\sigma/dQ^2_{\rm QE}$ associated with (I) muon reconstruction, (II) recoil reconstruction, (III) neutrino interaction models, (IV) final state interactions, (V) flux, and (VI) other sources. The rightmost column shows the total fractional systematic uncertainty due to all sources.

$Q^2_{\rm QE}$ (GeV^2)	I	II	III	IV	V	VI	Total
0.0–0.025	0.06	0.04	0.02	0.04	0.09	0.03	0.13
0.025–0.05	0.06	0.03	0.02	0.03	0.09	0.02	0.12
0.05–0.1	0.06	0.03	0.02	0.03	0.09	0.02	0.12
0.1–0.2	0.06	0.03	0.03	0.02	0.09	0.02	0.11
0.2–0.4	0.05	0.02	0.03	0.03	0.09	0.01	0.11
0.4–0.8	0.05	0.03	0.04	0.04	0.09	0.01	0.13
0.8–1.2	0.08	0.07	0.07	0.15	0.09	0.02	0.22
1.2–2.0	0.12	0.07	0.07	0.16	0.09	0.02	0.24

TABLE II. Flux-averaged differential cross sections and the fraction of the cross section in bins of $Q^2_{\rm QE}$. In each measurement, the first error is statistical and the second is systematic.

$Q^2_{\rm QE}$ (GeV^2)	Cross section (10^{-38} cm^2/GeV^2/neutron)	Fraction of Cross section (%)
0.0–0.025	$0.761 \pm 0.035 \pm 0.097$	$2.15 \pm 0.10 \pm 0.17$
0.025–0.05	$1.146 \pm 0.047 \pm 0.137$	$3.24 \pm 0.13 \pm 0.22$
0.05–0.1	$1.343 \pm 0.034 \pm 0.156$	$7.60 \pm 0.19 \pm 0.50$
0.1–0.2	$1.490 \pm 0.028 \pm 0.170$	$16.85 \pm 0.32 \pm 1.04$
0.2–0.4	$1.063 \pm 0.019 \pm 0.120$	$24.06 \pm 0.43 \pm 1.06$
0.4–0.8	$0.582 \pm 0.013 \pm 0.074$	$26.33 \pm 0.58 \pm 0.85$
0.8–1.2	$0.242 \pm 0.014 \pm 0.053$	$10.95 \pm 0.64 \pm 1.45$
1.2–2.0	$0.097 \pm 0.008 \pm 0.024$	$8.81 \pm 0.71 \pm 1.43$

knowledge of the flux. The saturation of ionization (dE/dx), parametrized by Birk's law and characterized by a factor of $(1 + k_B \times dE/dx)^{-1}$, leads to a recoil reconstruction uncertainty; this uncertainty is negligible for the antineutrino $d\sigma/dQ^2_{\rm QE}$ measurement but is important for the neutrino measurement. By studying stopping proton tracks in the MINERvA test beam detector we estimate $k_B = 0.13 \pm 0.04$ mm/MeV [39], and vary the ionization accordingly in the simulation to propagate the uncertainty.

The vertex energy distribution is sensitive to the multiplicity of low energy charged hadrons in the final state. Systematic uncertainties on this distribution are evaluated with the same methods used for the cross-section measurement. The largest uncertainties in the distribution come from the detector's response to protons (constrained by test beam measurements [39]), the Birk's law constant discussed above, and GENIE's final state interactions model. The latter is evaluated by varying the underlying model tuning parameters within their systematic uncertainties.

The measured differential cross section $d\sigma/dQ^2_{\rm QE}$ is shown in Table II and Fig. 3. Integrating over the flux from 1.5 to 10 GeV, we find [42] $\sigma = 0.93 \pm 0.01(\text{stat}) \pm 0.11(\text{syst}) \times 10^{-38}$ cm^2/neutron. Figures 3 and 4 and Table III compare the data to the RFG model in the GENIE event generator and a set of calculations made with the NuWro generator [19].

Different models of nuclear effects in quasielastic scattering lead to significant variations in the shape of $d\sigma/dQ^2$ from the expectation of the RFG model. In particular, correlations between nucleons not considered in the mean field RFG approach are predicted to contribute to the cross section at neutrino energies below 2 GeV [28–30]. Figure 4 compares the shape of the measured cross section to five different models of the quasielastic process on carbon. The GENIE prediction, based on a RFG nuclear model and dipole axial form factor with $M_A = 0.99$ GeV, is taken as a reference; the data and other models are normalized to have the same total cross section across the range shown before forming the ratio. The

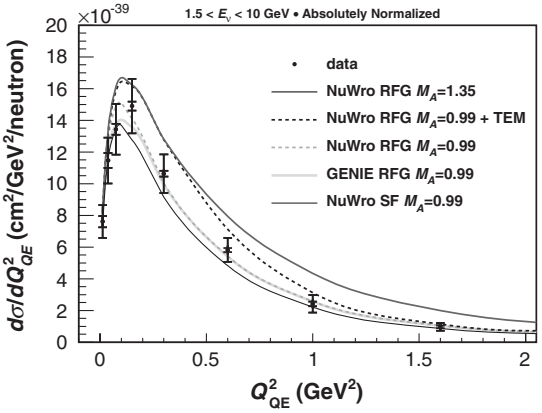

FIG. 3. Neutrino quasielastic cross section as a function of $Q^2_{\rm QE}$ compared with several different models of the interaction.

NuWro calculations utilize an axial-vector form factor parametrized with a dipole form that has one free parameter, the axial mass M_A, and also incorporate different corrections for the nuclear medium. There is little sensitivity to replacement of the Fermi gas with a SF model of the target nucleon energy-momentum relationship [31]. The neutrino data are marginally more compatible, at least in $Q^2_{\rm QE}$ shape, with a higher axial mass extracted from fits of the MiniBooNE neutrino quasielastic data in the RFG model ($M_A = 1.35$ GeV/c^2) [22] than with that extracted from deuterium data ($M_A = 0.99$ GeV/c^2). As with the corresponding antineutrino results [35], our data are in best agreement with a transverse enhancement model (TEM) with $M_A = 0.99$ GeV/c^2. This model implements an enhancement of the magnetic form factors of bound nucleons that has been extracted from electron-carbon scattering data [27], and is the only one of this type that is applicable at neutrino energies above 2 GeV. Table III shows a comparison using χ^2 values between the measured cross section and the five NuWro models considered.

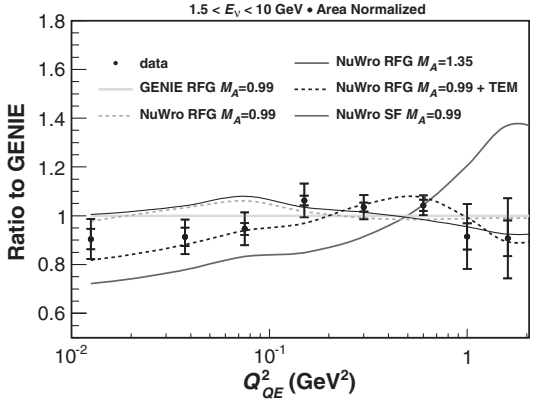

FIG. 4. Ratio between the measured neutrino $d\sigma/dQ^2_{\rm QE}$ shape in $Q^2_{\rm QE}$ and several different models, where the denominator is the GENIE default quasielastic cross section.

TABLE III. Comparisons between the measured $d\sigma/dQ^2_{\mathrm{QE}}$ (or its shape in Q^2_{QE}) and different models implemented using the NuWro neutrino event generator, expressed as χ^2 per degree of freedom (DOF) for eight (seven) degrees of freedom. The χ^2 computation in the table accounts for significant correlations between the data points caused by systematic uncertainties.

NuWro Model	RFG	RFG +TEM	RFG	SF
M_A (GeV/c^2)	0.99	0.99	1.35	0.99
Rate χ^2/DOF	3.5	2.4	3.7	2.8
Shape χ^2/DOF	4.1	1.7	2.1	3.8

Experience from electron quasielastic scattering on carbon suggests that multibody final states are dominated by initial-state np pairs [24,43,44]. This could lead to an expectation of final state pp pairs in neutrino quasielastic scattering and nn pairs in the analogous antineutrino channel. The vertex energy measurement, shown in Fig. 5, is sensitive to these effects. These data prefer the addition of a final state proton with less than 225 MeV kinetic energy in $25 \pm 1(\mathrm{stat}) \pm 9(\mathrm{syst})\%$ of the events. The corresponding result in the antineutrino mode [35], in contrast, prefers the removal of a final state proton in $10 \pm 1(\mathrm{stat}) \pm 7(\mathrm{syst})\%$ of the events. The systematic uncertainties for the two samples are positively correlated with a correlation coefficient of $+0.7$, implying that the observed difference is unlikely to be due to one of the systematic uncertainties considered. The systematic uncertainties are primarily from the detector response to protons and uncertainties in reactions in the target nucleus that absorb or create final state protons. Independent of models, elastic and inelastic nucleon reactions which might produce additional final state protons in the neutrino data should have analogous reactions in the antineutrino data, and the difference in the two results makes it unlikely that any modification of final state nucleon interactions can explain the discrepancy. Pion final state interactions (FSI), especially absorption, would produce more protons in the neutrino reaction and neutrons in the antineutrino reaction, but the associated uncertainties are included in the total systematic errors. The observed patterns in the neutrino and antineutrino channels, combined with the observation that electron quasielastic scattering with multinucleon final states in carbon produces primarily final state np pairs, suggests that an initial state of strongly correlated np pairs also may participate in the neutrino quasielastic interaction.

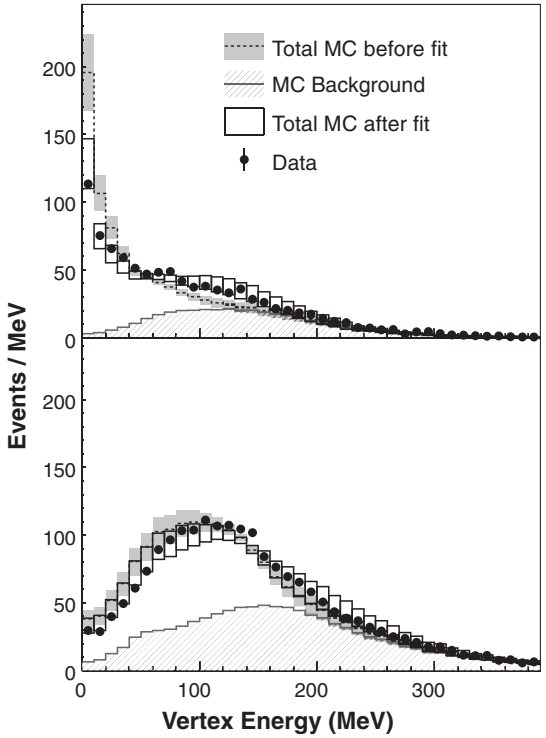

FIG. 5. Reconstructed vertex energy of events passing the selection criteria in the data (points with statistical errors) compared to the GENIE RFG model (shown with systematic errors) for $Q^2_{\mathrm{QE}} < 0.2$ GeV$^2/c^2$ (top) and for $Q^2_{\mathrm{QE}} > 0.2$ GeV$^2/c^2$ (bottom).

This work was supported by the Fermi National Accelerator Laboratory under United States Department of Energy (DOE) Office of High Energy Physics Contract No. DE-AC02-07CH11359 which included the MINERvA construction project. Construction support also was granted by the United States National Science Foundation (NSF) under Grant No. PHY-0619727 and by the University of Rochester. Support for participating scientists was provided by NSF and DOE (USA) by CAPES and CNPq (Brazil), by CoNaCyT (Mexico), by CONICYT (Chile), by CONCYTEC, DGI-PUCP, and IDI/IGI-UNI (Peru), by Latin American Center for Physics (CLAF) and by RAS and the Russian Ministry of Education and Science (Russia). We thank the MINOS Collaboration for use of its near detector data. Finally, we thank the staff of Fermilab for support of the beam line and detector.

*Deceased.
†Present address: Thomas Jefferson National Accelerator Facility, Newport News, VA 23606 USA.
‡Present address: Vrije Universiteit Brussel, Pleinlaan 2, B-1050 Brussels, Belgium.
§Also at Department of Physics, University of Antananarivo, Madagascar.
‖Present address: Temple University, Philadelphia, Pennsylvania 19122, USA.
¶Present address: Department of Physics, Royal Holloway, University of London, United Kingdom.

[1] A. A. Aguilar-Arevalo *et al.* (MiniBooNE Collaboration), Phys. Rev. Lett. **105**, 181801 (2010).
[2] A. A. Aguilar-Arevalo *et al.* (MiniBooNE Collaboration), Phys. Rev. Lett. **102**, 101802 (2009).

[3] K. Abe *et al.* (T2K Collaboration), Phys. Rev. Lett. **107**, 041801 (2011).
[4] D. S. Ayres *et al.* (NOvA Collaboration), arXiv:hep-ex/0503053.
[5] C. H. L. Smith, Phys. Rep. **3**, 261 (1972).
[6] R. Bradford, A. Bodek, H. S. Budd, and J. Arrington, Nucl. Phys. B, Proc. Suppl. **159**, 127 (2006).
[7] A. Bodek, S. Avvakumov, R. Bradford, and H. S. Budd, J. Phys. Conf. Ser. **110**, 082004 (2008).
[8] K. S. Kuzmin, V. V. Lyubushkin, and V. A. Naumov, Eur. Phys. J. C **54**, 517 (2008).
[9] M. Day and K. S. McFarland, Phys. Rev. D **86**, 053003 (2012).
[10] A. A. Aguilar-Arevalo *et al.* (MiniBooNE Collaboration), Nucl. Instrum. Methods Phys. Res., Sect. A **599**, 28 (2009).
[11] K. Abe *et al.* (T2K Collaboration), Nucl. Instrum. Methods Phys. Res., Sect. A **659**, 106 (2011).
[12] D. G. Michael *et al.* (MINOS Collaboration), Nucl. Instrum. Methods Phys. Res., Sect. A **596**, 190 (2008).
[13] H. Chen *et al.* (MicroBooNE Collaboration), FERMILAB, Report No. FERMILAB-PROPOSAL-0974, 2007.
[14] T. Akiri *et al.* (LBNE Collaboration), arXiv:1110.6249.
[15] R. A. Smith and E. J. Moniz, Nucl. Phys. **B43**, 605 (1972).
[16] A. Bodek and J. L. Ritchie, Phys. Rev. D **23**, 1070 (1981).
[17] C. Andreopoulos, A. Bell, D. Bhattacharya, F. Cavanna, J. Dobson, S. Dytman, H. Gallagher, P. Guzowski, R. Hatcher, P. Kehayias, A. Meregaglia, D. Naples, G. Pearce, A. Rubbia, M. Whalley, and T. Yang, Nucl. Instrum. Methods Phys. Res., Sect. A **614**, 87 (2010), Program version 2.6.2 used here.
[18] Y. Hayato, Acta Phys. Pol. B **40**, 2477 (2009).
[19] T. Golan, C. Juszczak, and J. T. Sobczyk, Phys. Rev. C **86**, 015505 (2012).
[20] O. Buss, T. Gaitanos, K. Gallmeister, H. van Hees, M. Kaskulov, O. Lalakulich, A. B. Larionov, T. Leitner, J. Weil, and U. Mosel, Phys. Rep. **512**, 1 (2012).
[21] O. Lalakulich, K. Gallmeister, and U. Mosel, Phys. Rev. C **86**, 014607 (2012).
[22] A. A. Aguilar-Arevalo *et al.* (MiniBooNE Collaboration), Phys. Rev. Lett. **100**, 032301 (2008).
[23] A. A. Aguilar-Arevalo *et al.* (MiniBooNE Collaboration), arXiv:1301.7067.
[24] R. Subedi, R. Shneor, P. Monaghan, B. D. Anderson, K. Aniol *et al.*, Science **320**, 1476 (2008).
[25] J. Carlson, J. Jourdan, R. Schiavilla, and I. Sick, Phys. Rev. C **65**, 024002 (2002).
[26] G. Shen, L. E. Marcucci, J. Carlson, S. Gandolfi, and R. Schiavilla, Phys. Rev. C **86**, 035503 (2012).
[27] A. Bodek, H. S. Budd, and M. E. Christy, Eur. Phys. J. C **71**, 1726 (2011).
[28] M. Martini, M. Ericson, G. Chanfray, and J. Marteau, Phys. Rev. C **81**, 045502 (2010).
[29] M. Martini and M. Ericson, Phys. Rev. C **87**, 065501 (2013).
[30] J. Nieves, M. Valverde, and M. J. V. Vacas, Phys. Rev. C **73**, 025504 (2006).
[31] O. Benhar, A. Fabrocini, S. Fantoni, and I. Sick, Nucl. Phys. **A579**, 493 (1994).
[32] J. Nieves, F. Sanchez, I. R. Simo, and M. J. V. Vacas, Phys. Rev. D **85**, 113008 (2012).
[33] O. Lalakulich, U. Mosel, and K. Gallmeister, Phys. Rev. C **86**, 054606 (2012).
[34] M. Martini, M. Ericson, and G. Chanfray, Phys. Rev. D **87**, 013009 (2013).
[35] L. Fields *et al.* (MINERvA Collaboration), preceding Letter, Phys. Rev. Lett. **111**, 022501 (2013).
[36] J. T. Sobczyk, Phys. Rev. C **86**, 015504 (2012).
[37] C. Alt *et al.* (NA49 Collaboration), Eur. Phys. J. C **49**, 897 (2007).
[38] The MINERvA scintillator tracking region is 95% CH and 5% other materials by weight.
[39] L. Aliaga *et al.* (MINERvA Collaboration), arXiv:1305.5199.
[40] Isolated energy depositions are created directly by the leading proton or by secondary hadronic interactions in the detector.
[41] T. Katori, Ph.D. thesis, Indiana University, 2008.
[42] See Supplemental Material at http://link.aps.org/supplemental/10.1103/PhysRevLett.111.022502 for the flux as a function of energy and for correlations of uncertainties among bins for the cross section and shape measurement.
[43] T. W. Donnelly and I. Sick, Phys. Rev. C **60**, 065502 (1999).
[44] M. Martini, M. Ericson, G. Chanfray, and J. Marteau, Phys. Rev. C **80**, 065501 (2009).